electronic reprint

Acta Crystallographica Section B
Structural Science
ISSN 0108-7681

Quantifying distortion from ideal closest-packing in a crystal structure with analysis and application

Richard M. Thompson and Robert T. Downs

Copyright © International Union of Crystallography

Author(s) of this paper may load this reprint on their own web site provided that this cover page is retained. Republication of this article or its storage in electronic databases or the like is not permitted without prior permission in writing from the IUCr.

Acta Crystallographica Section B
Structural Science
ISSN 0108-7681

Quantifying distortion from ideal closest-packing in a crystal structure with analysis and application

Richard M. Thompson* and Robert T. Downs

Department of Geosciences, University of Arizona, Tucson, Arizona 85721-0077, USA

Correspondence e-mail: thompson@geo.arizona.edu

Received 17 May 2000
Accepted 9 November 2000

A parameter, U_{cp}, that quantifies the distortion of the anion skeleton in a crystal from ideal closest-packing has been developed. It is a measure of the average isotropic displacement of the observed anions from their ideal equivalents. An ideal closest-packed structure can be fit to an observed structure by varying the radius of the ideal spheres, orientation and translation, such that U_{cp} is minimized. Ideal structures were fit to the $M1M2TO_4$ polymorphs, pyroxenes and kyanite. The distortions of these crystals were analyzed in terms of the two parameters, U_{cp} and the ideal radius. Changes in structures due to temperature, pressure and compositional effects were characterized in terms of these parameters.

1. Introduction

Traditionally, crystal chemistry has considered the analysis of anion–cation interactions to be the key to understanding the changes in crystal structure with pressure, temperature and composition (Pauling, 1940; Bragg *et al.*, 1965; Hazen & Finger, 1982). Crystal structures typically compress or expand by 'first-order' mechanisms that include angle-bending (*e.g.* Si—O—Si bending in quartz, SiO_2), bond distance changes (*e.g.* the Mg—O bond in MgO) and intermolecular distance changes (*e.g.* in a layer structure such as graphite; Hazen, 1999) and finally through dramatic phase transitions. Additionally, Hazen (1999) identifies the following mechanisms as being of lesser but still significant importance: cation polyhedral distortion, cation order–disorder reactions, electronic transitions and second-nearest neighbor cation–cation interactions.

However, theoretical work shows that anion–anion interactions play an important role in crystal chemistry (*cf.* Cohen, 1994, and references therein). It has long been thought that structures such as olivine, which clearly exhibit a distorted closest-packed arrangement of O atoms, become even more closest-packed with pressure (Kudoh & Takéuchi, 1985). In addition, an examination of pressure data for crystal structures which have not traditionally been considered to exhibit closest-packing, such as SiO_2 quartz (Glinneman *et al.*, 1992 – Fig. 1) and $CaFeSi_2O_6$, hedenbergite (Zhang *et al.*, 1997 – Fig. 2), suggests that their anions are also moving towards a closest-packed arrangement and this may be driving the observed angle-bending and bond-compression systematics (Hazen *et al.*, 1989; Sowa, 1988). These types of observation provide motivation to quantify the distortion of observed structures from their ideal closest-packed equivalents.

There have been several approaches to the characterization of the packing efficiency of observed structures. One strategy involves computing the relative volume of space occupied by

© 2001 International Union of Crystallography
Printed in Great Britain – all rights reserved

electronic reprint

the closest-packed atoms which are assumed to have fixed radii. Berry & Mason (1959) defined a packing index as the volume of ions/volume of unit cell × 10, while Scordari (1992) defined a packing coefficient, c_i, as the volume of the atoms/volume of the unit cell. Zoltai & Stout (1984) created a symmetrical packing index, SPI. This is an index similar to Berry & Mason (1959), with additional terms to compensate for the scaling of the structure due to interstitial cations. As the radii are assumed to be fixed, a scaling of structural volume requires that the closest-packed anions are either no longer in contact or are interpenetrating. We consider this algorithm to be deficient because it gives an SPI index of 65 for the more closest-packed Mg_2SiO_4 olivine and 72 for the poorly packed $CaFeSi_2O_6$ pyroxene. An ideal closest-packed structure has a Berry and Mason packing index of 7.4, a c_i of 0.74, and an SPI of 74. These indices become smaller with increasing distortion. Furthermore, these packing indices are not suitable for characterizing structures as a function of pressure or temperature since they use fixed effective radii.

Another approach to examining structural distortion is to analyze individual coordination polyhedra. Robinson *et al.* (1971) defined two measures of polyhedral distortion. Quadratic elongation, $\langle\lambda\rangle$, is a measure of the pairwise distortion in cation and anion separations. Bond-angle variance, σ^2, is the variance between the observed intrapolyhedral angles and the ideal angles. Regular polyhedra have a quadratic elongation of one and an angle variance of zero. These values increase with distortion. Robinson *et al.* (1971) showed that $\langle\lambda\rangle$ and σ^2 are linearly correlated for many silicates and isomorphic structures. However, Fleet (1976) showed that this correlation is not mandated by theory and does not hold true for all structure types. He suggested using quadratic elongation in conjunction with the mean-square relative deviation from the average bond length, Δ (Brown & Shannon, 1973).

Dollase (1974) fit a regular polyhedron to an observed polyhedron by minimizing the average distance between the observed anions and their ideal counterparts. This average distance is a one-parameter characterization of the distortion of the observed polyhedron. Yang *et al.* (1997) found that the polyhedral approach is not sufficient for understanding systematic trends at high pressure. In their study of the triclinic mineral kyanite, Al_2SiO_5, they discovered that some polyhedra become more regular while others become more distorted with pressure. Therefore, they created a new distortion parameter to characterize the entire structure. Their model minimized the average distance between all the observed O atoms in a 3 × 3 × 3 block of unit cells and their equivalents in an ideal cubic closest-packed arrangement. They found a systematic decrease in the distortion of kyanite from closest-packing that was consistent with the shape of the compressibility tensor. This model cannot be used for comparison between structure types, because different structures have different numbers of anions in their unit cells. Therefore, we have modified and generalized this approach in order to make these sorts of comparisons possible.

If an observed monoatomic structure or the anion skeleton in a polyatomic structure is considered to be a distorted closest-packed array of atoms or anions, then an ideally closest-packed arrangement of spheres can be matched to the observed structure in a one-to-one correspondence of ideal spheres to observed atoms or anions. Since the focus of our research is upper mantle oxide minerals, we will henceforth refer to anions rather than atoms. The radius of the ideal spheres and the orientation and origin of the ideal arrangement can be varied to make a closest fit to the observed structure. A distortion parameter, U_{cp}, is defined to measure the average mean-squared displacement of the ideal spheres from their observed equivalents

$$U_{cp} = \sum_{j=1}^{\#anions} [R_j^2(\text{observed} - \text{ideal})/\#\text{anions}], \qquad (1)$$

where R_j(observed − ideal) is the distance from the jth observed anion to its ideal equivalent. The fit is accomplished by minimizing the value of this distortion parameter. We intend to use U_{cp} and the ideal sphere radius to analyze structural data sets as functions of pressure, temperature and composition, and to formulate and test hypotheses about compression mechanisms. We expect, for instance, that a pressure-induced volume change would correspond to a

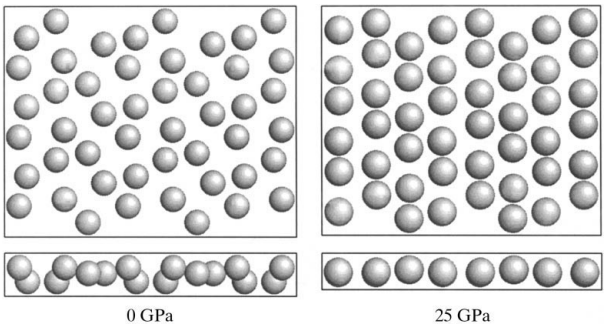

Figure 1
A monolayer of anions in the tetrahedral framework quartz, SiO_2, viewed down [110] and on edge. Glinneman *et al.*'s (1992) data was extrapolated to 25 GPa, the pressure at which quartz becomes amorphous at room temperature.

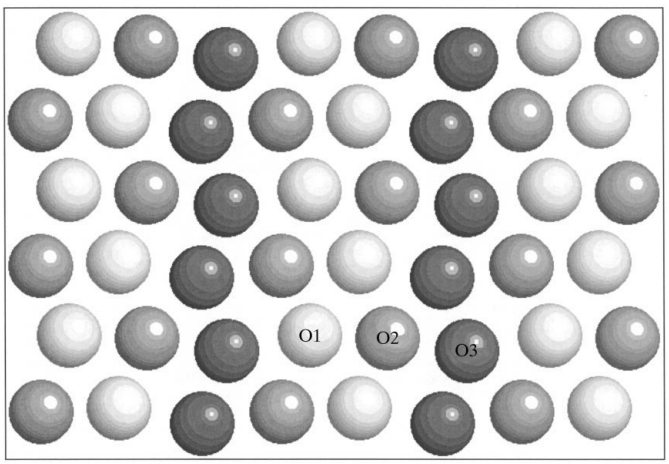

Figure 2
A monolayer of anions in $CaFeSi_2O_6$ hedenbergite, viewed down **a***. Data is extrapolated to 50 GPa from Zhang *et al.* (1997).

electronic reprint

decrease in both the radius of the ideal sphere and the distortion parameter. However, it seems reasonable that a highly distorted structure could decrease its volume by reducing its distortion without a change in the ideal radius, while a structure observed to be close to ideal would primarily exhibit a decrease in radius. In contrast, we expect these parameters to increase with temperature.

2. Parameter design and relevant closest-packing background

We wanted U_{cp} to express the distortion of the anion skeleton in an observed crystal from ideally closest-packed and to be comparable across different structures, including the two standard packing arrangements, cubic and hexagonal closest-packing. As will be shown in detail in §6 of this paper, the average distance from an observed anion to its ideal equivalent sphere can increase with the number of anions being fit, so there is no absolute quantitative measure of this type of distortion for a structure. Thus, we had to find a way to chose a portion of any given crystal that would be comparable to a portion in any other crystal. This was accomplished by selecting a spherical volume of ideal space containing 675 spheres in the *CCP* (cubic closest-packing) case, and 677 in the *HCP* (hexagonal closest-packing) case.

The choice of these numbers is a result of the different radial distributions of spheres in the two cases. Starting from a single sphere in either arrangement, and moving outward radially, spheres are added in shells at distances determined by the ideal sphere radius. On the one hand, the spheres in *CCP* are located on inversion centers so that a given spherical volume of space contains a symmetrical cluster of spheres. On the other hand, in *HCP* the spheres are not located on inversion centers so that the cluster of spheres in a spherical volume of space has a slightly lopsided distribution. A given spherical volume of *HCP* space contains about twice as many shells, each with about half as many spheres, as the same volume of *CCP* space (Patterson & Kasper, 1959). Picking 675 spheres for *CCP* and 677 for *HCP* allows reasonable comparison between the two types of arrangements. Removing the two extra spheres from the outer shell of the *HCP* arrangements is problematic because the choice of the two is unique and affects the value of U_{cp}, albeit very slightly. The calculation to determine which two to remove in order to find the minimum value of U_{cp} is unreasonably time consuming. For instance, it takes 10 s to run through the calculation of U_{cp} once for $LiScSiO_4$ on our 550 Mhz PC. Obtaining the true minimum for this structure, with removal of two spheres, would take at least $8 \times 3 \times 10 \times 227 \times 226/2 =$ 6 156 240 s or 71 d.

3. Algorithm fundamentals

Our implementation of the algorithm is currently only equipped to analyze structures based on cubic or hexagonal closest-packing. Other stacking sequences are not accommodated. The ideal cubic closest-packed arrangement is constructed using a rhombohedral basis $a = b = c = 2r$, $\alpha = \beta = \gamma = 60^\circ$, where r is the radius of a sphere in the arrangement. The ideal hexagonal closest-packed arrangement uses the basis $a = b = 2r$, $c = 4(6)^{1/2}r/3$, $\alpha = \beta = 90^\circ$, $\gamma = 120^\circ$, with spheres at {[0,0,0], [2/3,1/3,1/2]}.

At the heart of the algorithm is the creation of an ideally closest-packed arrangement of spheres and the correct assignment of a one-to-one correspondence between these spheres and the anions in an observed crystal structure. This is accomplished by creating a transformation matrix that takes the coordinates of an observed anion from a direct space basis to a rhombohedral (*CCP*) or hexagonal (*HCP*) basis. The closest-packing based coordinates are then modified to be ideal by rounding to the nearest integer for *CCP* or the nearest possible ideal *HCP* coordinates for *HCP* ([i,j,k] or [2/3 + i, 1/3 + j, $\frac{1}{2}$ + k], where $i, j, k \in Z$).

To obtain this transformation matrix, the algorithm isolates an anion and its 12 nearest neighbors. It goes through all possible combinations of these neighbors, looking for groups of three that form the base of a tetrahedron that has the central anion as its other corner. A vector from the central anion through the middle of the base is a possible stacking vector for closest-packed monolayers. In the *CCP* case, it may be one of eight such stacking vectors. In the *HCP* case, there should be two valid stacking vectors out of eight possibilities.

Once a possible stacking vector has been found, the transformation matrix can be created. In the *CCP* case, the algorithm takes the Cartesian coordinates of the three neighbors forming the tetrahedron and treats them as vectors, $\{\mathbf{a}_c, \mathbf{b}_c, \mathbf{c}_c\}$, originating from the central anion. These three vectors form a distorted rhombohedral basis for the structure and therefore form the columns of a transformation matrix from rhombohedral to Cartesian space

$$T_{\mathrm{R\_to\_C}} = [\mathbf{a}_c|\mathbf{b}_c|\mathbf{c}_c].$$

The values of the transformation matrix can be further refined using all 12 nearest neighbors in a least-squares method. A transformation matrix from direct space to the distorted rhombohedral space, $T_{\mathrm{D\_to\_R}}$, is obtained by multiplying the direct to Cartesian transformation matrix, $A_{\mathrm{D\_to\_C}}$, for the structure by the inverse of $T_{\mathrm{R\_to\_C}}$,

$$T_{\mathrm{D\_to\_R}} = A_{\mathrm{D\_to\_C}} \times (T_{\mathrm{R\_to\_C}})^{-1}.$$

Transforming each anion in the unit cell into distorted rhombohedral coordinates and rounding these coordinates to nearest integers gives ideal rhombohedral space coordinates, *i.e.* coordinates of ideally *CCP* equivalents. A transformation matrix is constructed in a similar manner for the *HCP* case; details can be found in Thompson (2000).

We store Cartesian space coordinates of the observed anions in one array, $[\mathbf{x_O}]_C$, and the rhombohedral or hexagonal coordinates of the ideal equivalent spheres with corresponding indices in a second array, $[\mathbf{x_I}]_{CP}$. The ideal coordinates are then transformed to a Cartesian basis with

electronic reprint

Table 1
Refined values of ideal radius and U_{cp} for selected crystal structures.

Mineral	GPa	T (K)	Rad	U_{cp}
Chrysoberyl	0		1.36177	0.02194
	1.4		1.35948	0.02380
	3.15		1.35632	0.02029
	4		1.35495	0.02288
	5.4		1.35218	0.02205
	6.25		1.35082	0.02023
Co_2SiO_4 – olivine, Morimoto & Güven (1970)			1.48369	0.08917
Co_2SiO_4 – wadsleyite			1.45101	0.04914
Co_2SiO_4 – spinel w/o site			1.43861	0.01335
Co_2SiO_4 – spinel w site oc			1.43861	0.01401
Fayalite, Kudoh & Takeda (1986)	0		1.50433	0.11705
	4.9		1.48840	0.09775
	6.7		1.48227	0.10552
	9.3		1.47246	0.10189
	11.7		1.46861	0.20784
	14		1.45824	0.22081
Fayalite, Hazen (1977), in cell	0		1.50254	0.11127
	3.1		1.48996	0.22282
	4.2		1.48526	0.16162
Fayalite, Hazen, in air	0	296	1.50236	0.12274
Fayalite, Hazen	0	77	1.50007	0.11300
Fayalite, Smyth (1975)		293	1.50243	0.11656
		573	1.50526	0.12072
		873	1.51051	0.12396
		1123	1.51625	0.13399
Forsterite, Takéuchi *et al.* (1984)		571	1.47278	0.07552
		856	1.47618	0.07763
		1076	1.47982	0.08085
		1246	1.48289	0.08252
		1496	1.48884	0.08841
		1596	1.49153	0.09165
		1756	1.49618	0.09523
		1946	1.50135	0.10328
		2146	1.50566	0.10790
Forsterite, Kudoh & Takéuchi (1985)	3.1	569	1.46186	0.07681
	4.7	569	1.45540	0.06958
	5.3	569	1.45325	0.06958
	7.9	569	1.44447	0.07146
	8.6	569	1.44187	0.06981
	11.1	569	1.43643	0.08563
	14.9	569	1.42305	0.07816
Forsterite 51, tephroite 49, Francis & Ribbe (1980)			1.50407	0.10870
Forsterite 09, tephroite 91			1.52668	0.13029
Forsterite, Hazen (1976)	0	350	1.47192	0.07655
	0	569	1.47376	0.07561
	0	1169	1.47843	0.08650
	0	1221	1.48387	0.08791
	0	1546	1.49258	0.09571
	0	569	1.47376	0.07561
	2	569	1.46539	0.07940
	4	569	1.46372	0.07104
	5	569	1.45709	0.09650
Glaucochroite, Lager & Meagher (1978)		571	1.57848	0.27157
		846	1.58223	0.27932
		1146	1.58752	0.29061
		1346	1.59126	0.28778
Hortonolite, Hazen (1977)	0	569	1.49391	0.10007
	0	846	1.49855	0.10714
	0	1146	1.50357	0.10746
	0	1446	1.50953	0.14043
Hortonolite, Brown & Prewitt (1973)	0	570	1.48591	0.08559
	0	921	1.49022	0.08903
	0	1256	1.49455	0.09625
$LiScSiO_4$, *XTAL*0, Hazen *et al.* (1996)	0		1.49034	0.10209
$LiScSiO_4$, *XTAL*1	0.06		1.49120	0.10321
$LiScSiO_4$, *XTAL*2	0.21		1.49135	0.10021
$LiScSiO_4$, *XTAL*2	0.23		1.49083	0.09704
$LiScSiO_4$, *XTAL*2	0.99		1.48711	0.09706

Table 1 (continued)

Mineral	GPa	T (K)	Rad	U_{cp}
$LiScSiO_4$, *XTAL*1	1.46		1.48497	0.09526
$LiScSiO_4$, *XTAL*2	2.17		1.48286	0.08948
$LiScSiO_4$, *XTAL*2	3.02		1.47920	0.08565
$LiScSiO_4$, *XTAL*2	3.72		1.47660	0.08246
$LiScSiO_4$, *XTAL*1	4.26		1.47441	0.08229
$LiScSiO_4$, *XTAL*2	4.51		1.47332	0.07939
$LiScSiO_4$, *XTAL*2	5.15		1.47061	0.07557
Mg_2SiO_4 – olivine, Takéuchi		298	1.47278	0.07552
Wadsleyite, Fe00	0		1.43894	0.03877
Spinel, Mg_2SiO_4, Hazen			1.42675	0.00675
Monticellite, Sharp *et al.* (1987)	0		1.55800	0.29462
	1.11		1.55306	0.27877
	2.07		1.54809	0.26679
	2.91		1.54485	0.26723
	4.12		1.53957	0.26233
	5.3		1.53573	0.25058
	6.17		1.53251	0.24606
Monticellite, Lager & Meagher (1978)		298	1.55886	0.28977
		608	1.56368	0.30458
		888	1.56876	0.30913
		1068	1.57228	0.31626
Ni-olivine, Lager & Meagher (1978)		298	1.46164	0.06467
		673	1.46672	0.06676
		873	1.47119	0.06985
		1173	1.47617	0.07218
Spinel, Ni_2SiO_4, Finger *et al.* (1979)	0	296	1.42203	0.00722
	1.12		1.41955	0.00696
	2.25		1.41722	0.00671
	3.1		1.41573	0.00647
	3.65		1.41485	0.00581
	3.82		1.41446	0.00480
Spinel, Fe_2SiO_4, Finger *et al.* (1979)			1.45593	0.01685
Spinel, Mg_2SiO_4, Hazen *et al.* (1993)			1.42675	0.00675
Spinel, Mg21, Fe79, Hazen *et al.* (1993)			1.45061	0.01367
Spinel, Mg21, Fe79, Hazen *et al.* (1993)			0.01441	0.01441
Spinel, Mg38, Fe62, Hazen *et al.* (1993)			1.44538	0.01291
Spinel, Mg_2TiO_4, Wechsler & Von Dreele (1989)			1.49157	0.02349
Olivine, Mg_2TiO4, Wechsler			1.49163	0.03358
Spinel, Ni_2SiO_4, Yagi *et al.* (1974)			1.42199	0.00770
Spinel, Fe_2SiO_4, Yagi			1.45558	0.01721
Spinel, Fe_2SiO_4, Marumo *et al.* (1977)			1.45558	0.01691
Spinel, Co_2SiO_4, Marumo			1.43896	0.01187
Wadsleyite, Fe25, Hazen *et al.* (2001)	0		1.44546	0.04388
	2.72		1.43842	0.03834
	5.23		1.43231	0.03508
	6.8		1.42863	0.03354
	8.49		1.42528	0.03186
	10.1		1.42188	0.03039
Wadsleyite, Fe00, Hazen *et al.* (2001)	0		1.43894	0.03877
	2.72		1.43180	0.03623
	5.23		1.42566	0.03182
	6.8		1.42213	0.03115
	8.49		1.41839	0.02880
	10.1		1.41235	0.02655
$Ca_{40}Mg_{60}Si_2O_6$, Benna *et al.* (1990)		–130	1.47828	0.59625
		298	1.47817	0.61882
		673	1.48408	0.66024
		973	1.48840	0.68482
Clinoenstatite, Angel *et al.* (1989)			1.46954	1.04788
Diopside, Levien & Prewitt (1981)	0		1.48116	0.58509
	2.36		1.47114	0.54056
	3.52		1.46679	0.52024
	4.55		1.46291	0.50445
	5.3		1.46003	0.49406
Diopside, Clark *et al.* (1969)			1.48042	0.56686
Diopside, Cameron *et al.* (1993)		297	1.48037	0.56698

electronic reprint

Table 1 (continued)

Mineral	GPa	T (K)	Rad	U_{cp}
		673	1.48728	0.60678
		973	1.49175	0.62426
		1123	1.49384	0.63237
		1273	1.49688	0.63732
Diopside, Finger & Ohashi (1976)		973	1.49218	0.62333
Fassaite, Hazen & Finger (1977)	0		1.48115	0.58137
	1.5		1.47400	0.56123
	2.9		1.46725	0.52987
	4.5		1.46067	0.51123
Ferrosilite, Hugh-Jones *et al.* (1994)	0		1.47985	0.93157
	1.87		1.45601	0.20393
	0		1.47985	0.93157
	1.6			0.91000
	1.6			0.20393
	1.87		1.45601	0.20393
	1.87		1.45672	0.20727
	1.87		1.45624	0.20503
Hedenbergite, Zhang *et al.* (1997)	0		1.49258	0.48821
	1.19		1.48753	0.46016
	2.15		1.48409	0.44212
	2.75		1.48086	0.42918
	3.65		1.47799	0.41497
	4.44		1.47457	0.40233
	4.83		1.47324	0.40018
	5.3		1.47175	0.38755
	6.45		1.46798	0.37953
	7.63		1.46343	0.36608
	8.75		1.45972	0.35570
	9.97		1.45596	0.35168
Hedenbergite, Cameron *et al.* (1973)		297	1.49339	0.48677
		673	1.49832	0.52453
		873	1.50124	0.54504
		1073	1.50381	0.55976
		1173	1.50599	0.56841
		1273	1.50749	0.57790
Kanoite, Arlt *et al.* (1998)	0			0.98583
	5.2		1.43920	0.17123
	0	298	1.47212	0.98583
	5.06	298	1.47212	0.90000
	5.06	298	1.47212	0.17123
	5.2		1.43920	0.17123
	5.2		1.44006	0.17519
	5.2		1.43946	0.17276
i.e.n.a.c.		473	1.47759	1.04749
Pigeonite, Morimoto & Güven (1970)			1.47399	1.10017
			1.47473	0.98718
Kyanite, Yang *et al.* (1997)	0		1.37405	0.06620
	1.35		1.37089	0.06385
	2.54		1.36837	0.06312
	3.73		1.36550	0.06157
	4.56		1.36370	0.06082
Kyanite, Winter & Ghose (1979)		297	1.37450	0.06539
		673	1.37874	0.06981
		873	1.38131	0.06972

transformation matrix $A_{CP\_to\_C}$, rotated in space with a unitary rotation matrix R, and translated by a vector $\mathbf{t}$

$$RA_{CP\_to\_C}[\mathbf{x_l}]_{CP} + \mathbf{t}.$$

We parameterize R in terms of a unit length vector, $\mathbf{l}$, about which a rotation of magnitude ρ takes place. We then vary seven parameters (ρ, the two components of $\mathbf{l}$, $\mathbf{t}$ and r) to allow the ideal arrangement to achieve any orientation, origin and scale. U_{cp} is computed using (1) and its value minimized based on a quasi-Newton method that uses a model trust region with a double dogleg as described in Dennis & Schnabel (1983) and coded by Lee Johnson and Monte Boisen of the Math Department at Virginia Tech. This minimizer does not require derivatives.

4. Data sets

We ran selected structural data sets, some at P and T, for the $M1M2TO_4$ polymorphs, pyroxenes and kyanite through the algorithm, including: $Mg_{1.425}Cr_{0.611}Si_{1.964}O_6$, clinopyroxene (Angel *et al.*, 1989), $Mn_{0.9}Mg_{1.1}Si_2O_6$, kanoite (Arlt *et al.*, 1998), $Ca_{0.8}Mg_{1.2}Si_2O_6$, clinopyroxene (Benna *et al.*, 1990), $(Mg_{1.4}Fe_{0.6})SiO_4$, hortonolite (Brown & Prewitt, 1973), $CaMgSi_2O_6$, diopside, and $CaFeSi_2O_6$, hedenbergite (Cameron *et al.*, 1973), $CaMgSi_2O_6$, diopside (Clark *et al.*, 1969), $CaMgSi_2O_6$, diopside (Finger & Ohashi, 1976), Fe_2SiO_4 and Ni_2SiO_4, spinel (Finger *et al.*, 1979), $Mg_{1.02}Mn_{0.98}SiO_4$, olivine, and $Mg_{0.18}Mn_{1.92}SiO_4$ tephroite (Francis & Ribbe, 1980), Mg_2SiO_4 forsterite (Hazen, 1976), Fe_2SiO_4, fayalite, and $Mg_{0.75}Fe_{1.10}Mn_{0.15}SiO_4$, hortonolite (Hazen, 1977), $BeAl_2O_4$, chrysoberyl (Hazen, 1987), $(Ca_{0.87}Mg_{0.59}Fe^{2+}_{0.21}Ti^{4+}_{0.06}Al_{0.17})(Si_{1.72}Al_{0.17})O_6$, fassaite (Hazen & Finger, 1977), $(Mg_xFe_{1-x})_2SiO_4$, spinel (Hazen *et al.*, 1993), $LiScSiO_4$, olivine (Hazen *et al.*, 1996), $(Mg_xFe_{1-x})_2SiO_4$, wadsleyite (Hazen *et al.*, 2001), $FeSiO_3$, ferrosilite (Hugh-Jones *et al.*, 1994), Fe_2SiO_4, fayalite (Kudoh & Takeda, 1986), Mg_2SiO_4, forsterite (Kudoh & Takéuchi, 1985), $CaMnSiO_4$, glaucochroite, $CaMgSiO_4$, monticellite, and Ni_2SiO_4, olivine (Lager & Meagher, 1978), $CaMgSi_2O_6$, diopside (Levien & Prewitt, 1981), Fe_2SiO_4 and Co_2SiO_4, spinel (Marumo *et al.*, 1977), $(Mg_{0.39}Fe_{0.52}Ca_{0.09})SiO_3$, pigeonite (Morimoto & Güven, 1970), Co_2SiO_4, olivine, wadsleyite, and spinel (Morimoto *et al.*, 1974), $CaMgSiO_4$, monticellite (Sharp *et al.*, 1987), Fe_2SiO_4, fayalite (Smyth, 1975), Mg_2SiO_4, forsterite (Takéuchi *et al.*, 1984), Mg_2TiO_4, olivine and spinel (Wechsler & Von Dreele, 1989), Al_2SiO_5, kyanite (Winter & Ghose, 1979), Fe_2SiO_4 and Ni_2SiO_4, spinel (Yagi *et al.*, 1974), Al_2SiO_5, kyanite (Yang *et al.*, 1997), $CaFeSi_2O_6$, hedenbergite (Zhang *et al.*, 1997). The fit parameter, U_{cp}, and the ideal radius, r, for each of these data sets are reported in Table 1.

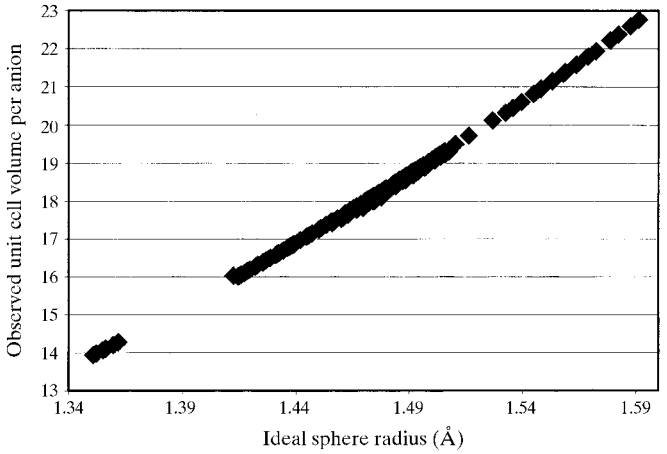

Figure 3
Plot showing that the ideal radius r can be thought of as a proxy for volume of space per anion in the observed structure.

electronic reprint

5. Analysis of ideal radius

The fitted values of the ideal radius, r, for room-conditions data are not constant, but range from 1.36 Å in chrysoberyl to 1.58 Å in glaucochroite (Table 1). To explain this variation in r, we show in Fig. 3 a plot of the volume of the observed unit cell divided by the number of anions in that unit cell *versus* the radius of the spheres in the ideal equivalent structure for all the data sets we analyzed. A nearly linear relationship is observed, demonstrating that r is a proxy for volume per anion.

To obtain the exact relationship, we divide the ideal sphere volume by the fraction of space occupied by a sphere, $(2)^{1/2}\pi/6$ (Patterson & Kasper, 1959), giving the volume of ideal structure per ideal sphere = $(4\pi r^3/3)/(2^{1/2}\pi/6) = 4(2)^{1/2}r^3$. Regressing the observed volume per anion against $4(2)^{1/2}r^3$ for all of our data gives

observed volume per anion $= 0.993\,(2) \times 4(2)^{1/2}r^3 + 0.10\,(3)$.

The slope is not exactly one and the intercept is not exactly zero, because the ideal unit cell is rarely the same size as the observed unit cell. The variation of r as a function of pressure and temperature follows this trend, with the change in r dependent only upon the change in volume. The packing indices described in §1 are modified measures of the fraction of space occupied by anions. Since the fraction of space occupied by anions is directly related to the volume per anion, r essentially contains the same information as the packing indices.

6. Analysis of U_{cp}

The room-condition variation of U_{cp} is a strong function of structure type. U_{cp} appears to be correlated with the pressure stability field for the $M1M2SiO_4$ polymorphs. The smallest values were recorded for spinels, ranging from 0.01 to 0.02 Å^2. U_{cp} values for wadsleyite were in the neighborhood of 0.04 Å^2. Silicate olivines ranged from 0.08 to 0.3 Å^2. Pyroxenes are more distorted than the $M1M2SiO_4$ polymorphs. Values for $C2/c$ pyroxenes ranged from 0.5 to 0.6 Å^2, while the $P2_1/c$ pyroxenes exhibited values near 1. Successful refinement of pyroxene data was difficult due to the high structural distortion. Improvement of our algorithm will be required to analyze structures that are more distorted than the pyroxenes.

Fig. 4 shows the variation in U_{cp} with pressure and temperature for structures in our data set. The dashed lines show how U_{cp} would vary due only to scaling of cell parameters. The trends for the individual structures are diverging from these lines. This means that the anions are shifting their relative positions to move closer to (pressure) or further from (temperature) closest-packed symmetry. An examination of Fig. 4(*a*) indicates that structures with high initial values of U_{cp} exhibit a greater rate of change of U_{cp} with pressure. We regressed each of the data sets linearly and plotted the refined initial U_{cp} against $-dU_{cp}/dP$ (Fig. 5). Regressing this data gives the following relation $U_{cp} = 0.00\,(1) - 34\,(2) \times dU_{cp}/dP$

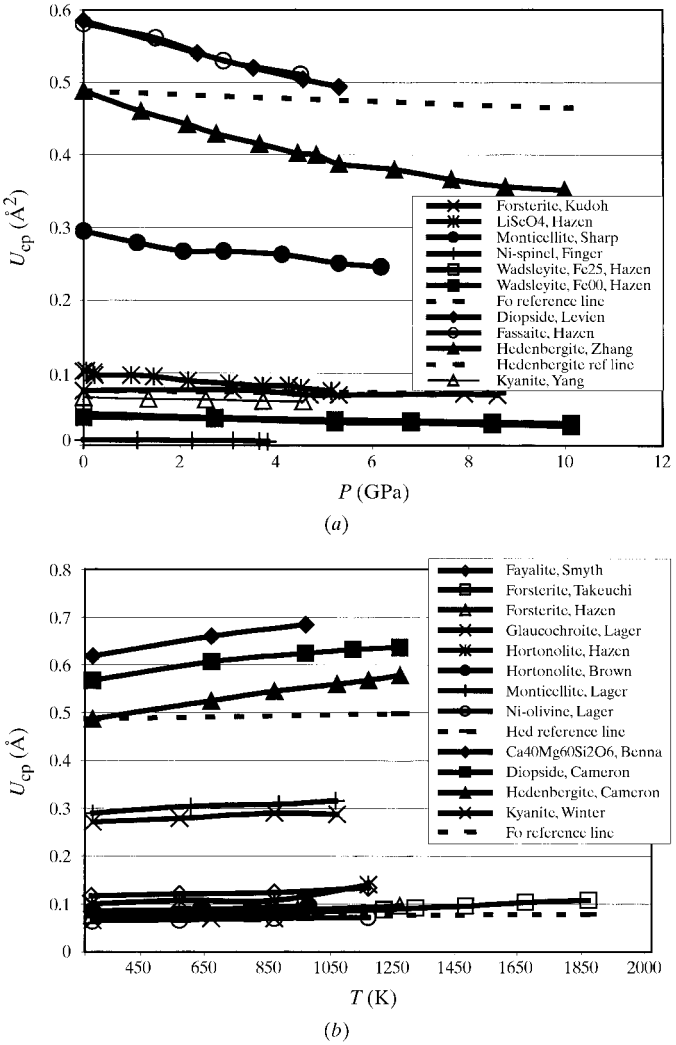

Figure 4
Scatterplots of U_{eq} as a function of (*a*) pressure and (*b*) temperature. Solid lines joining data points have been inserted as a guide for the eye. Dashed lines illustrate how U_{eq} would vary due only to proportional compression or expansion of cell parameters. Deviation from dashed lines demonstrates the contribution to U_{cp} resulting from positional distortion.

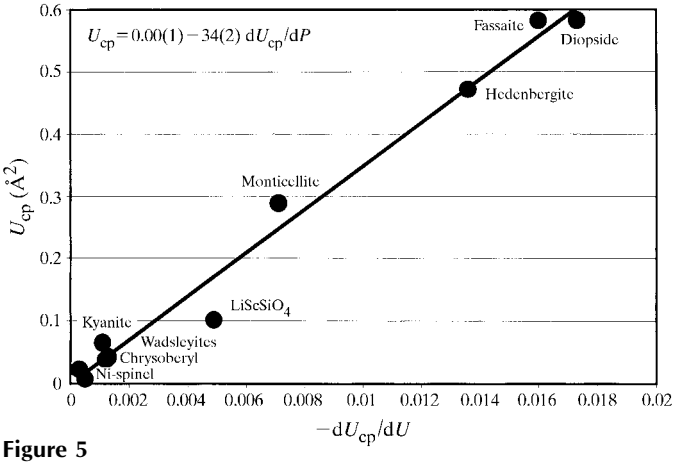

Figure 5
A scatterplot of U_{cp} as a function of its pressure derivative. This figure illustrates that the greater the distortion, the greater the effect of pressure. The solid line represents a linear fit.

electronic reprint

Table 2
The dependence of U_{cp} on the number of anions and spheres in the arrangements being fit can vary dramatically from crystal to crystal.

No. of anions being fit	U_{cp} for $LiScSiO_4$	U_{cp} for $CaMgSiO_4$
19	0.10145	0.11953
227	0.09491	0.19686
677	0.10209	0.29462
991	0.10652	0.35429

(R^2 = 0.983). A similar, although not so well defined, trend exists for U_{cp} and its temperature derivative.

Distortion from ideal closest-packing appears to be the result of two mechanisms: distortion in (i) the cell parameters and (ii) positional parameters. We analyzed the effects of these mechanisms by looking at the distribution of displacement vectors for each of the anions in the observed structures. We define a displacement vector as the vector originating at a sphere in the best-fit ideal arrangement and terminating at its corresponding observed anion.

If we know the structural parameters for an ideal closest-packed equivalent to an observed structure, then we can demonstrate the effects of the two different distortion mechanisms in that structure. For example, Fig. 6(*a*) shows the distribution of displacement vectors for $LiScSiO_4$ olivine. Fig. 6(*b*) shows the distribution for a theoretical crystal created from the observed cell parameters of $LiScSiO_4$ and the positional parameters of an ideal closest-packed olivine. Fig. 6(*c*) shows the distribution for a theoretical crystal created from the observed positional parameters of $LiScSiO_4$ and the cell parameters of an ideal closest-packed olivine. The distribution for the observed structure clearly results from a combination of the two distortion mechanisms. This type of observation holds for the other structures we have examined as well. Since cubic structures are characterized by a single cell parameter, all of their distortion is due to positional deviation from ideal.

The fact that U_{cp} is proportional to the number of anions being fit is a result due entirely to cell parameter distortion. A theoretical structure with ideal cell parameter ratios but with distorted positional parameters will have a value for U_{cp} that is independent of the number of anions outside the unit cell. The edges of the unit cells in a crystal with ideal cell parameters will match exactly with the edges of its ideal equivalent. The position of the ideal equivalent spheres relative to the observed anions will thus be identical in every unit cell and therefore U_{cp} will remain fixed.

A comparison of the olivine structures, $LiScSiO_4$ and $CaMgSiO_4$, demonstrates the effect of these mechanisms on the value of U_{cp}. For an ideal olivine, the cell parameter ratios are $a/b = 2^{1/2}3 = 0.47140$ and $a/c = 6^{1/2}3 = 0.81650$ (Brown, 1982). The cell parameter ratios for $LiScSiO_4$ are quite close to ideal, a/b = 0.46175 and a/c = 0.80751, while those for $CaMgSiO_4$ are more distorted, a/b = 0.43413 and a/c = 0.75552. Consequently, by varying the number of anions being fit, we see that U_{cp} for $LiScSiO_4$ is quite stable, but increases rapidly for $CaMgSiO_4$ (Table 2).

7. Correlation between U_{cp} and radius

Several distinct trends are exhibited between the ideal radius and the distortion parameter for the $M1M2SiO_4$ polymorphs (Fig. 7). The values of U_{cp} and r obtained for individual structures as a function of temperature and pressure are positively correlated. It is observed that steep slopes are associated with small values of r and U_{cp}, while shallow slopes are associated with large values of r and U_{cp}. This appears to be related to the two types of distortion. For structures with small values of U_{cp}, the change in distortion is effectively due to scaling of cell parameters. The change in U_{cp} for more distorted structures is usually dominated by positional distortion, as demonstrated in Fig. 4. We have added dashed lines to Fig. 4 which show how U_{cp} would vary with pressure due only to the scaling of cell parameters for two structures, $CaFeSi_2O_6$, hedenbergite, and Mg_2SiO_4, forsterite. Similarly, we have added a solid line to Fig. 7 that shows how r would vary with U_{cp} due only to the scaling of cell parameters for forsterite.

Two trends stand out when studying Fig. 7. The first is an extension of the aforementioned correlation between U_{cp} and

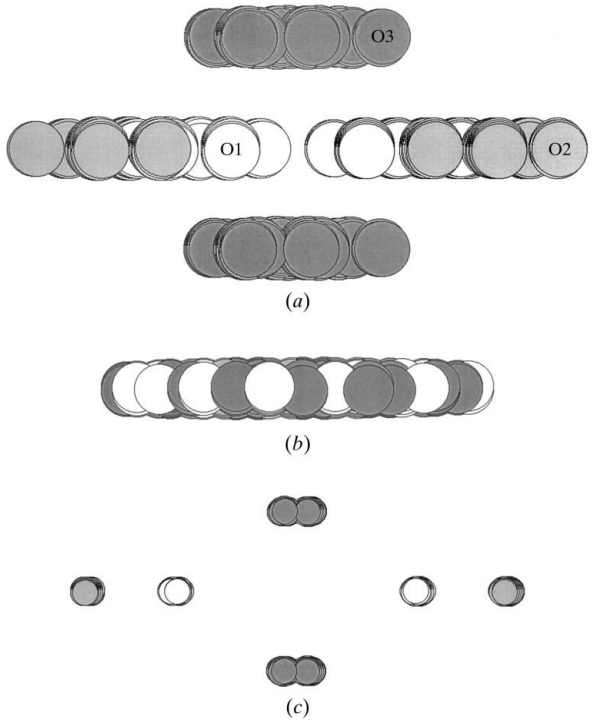

Figure 6
(*a*) Represents the displacement of observed anions from their ideal positions for $LiScSiO_4$ (Hazen *et al.*, 1996) as viewed down the *a* axis. The origin for each atom is at the center of the figure. The O1 and O2 atoms are displaced only in the *ab* plane, while O3 atoms are also displaced parallel to **c**. Note that the circles do not represent the locations of anions in the crystal structure. (*b*) Demonstrates the effect of distortion due only to cell parameters by showing the displacement distribution for a theoretical crystal with the cell parameters observed for $LiScSiO_4$ and the positional parameters of an ideally closest-packed olivine. (*c*) This figure demonstrates the effect of distortion due only to positional parameters by showing the displacement distribution for a theoretical crystal with the observed positional parameters of $LiScSiO_4$ and the cell parameters of an ideally closest-packed olivine.

electronic reprint

the pressure stability fields of the structures into r–U_{cp} space. The leftmost data set is from nickel spinel, the next two overlapping data sets are from wadsleyites and the rest of the data points are from olivine structures.

A final trend is related to the distribution of data for the olivine structures. Most of the data fall on a single trend in the neighborhood of $1.44 \leq r \leq 1.52$ and $0.07 \leq U_{cp} \leq 0.15$. The glaucochroite and montecellite structures have significantly larger values of r and U_{cp}. These distributions appear to be related to the sizes of the cations in the two octahedral sites. In the olivine structure, a mismatch exists due to the difference in sizes between the tetrahedral and octahedral site cations. Since the silicate tetrahedral volume remains essentially constant despite pressure, temperature and compositional changes, and the tetrahedra share edges with the octahedra, increasing octahedral cation size increases the distortion of the structure more than just scaling cell parameters. A further mismatch is created if there are differences between the sizes of the two octahedral sites. In Fig. 7 we have indicated the sizes of the two octahedral cations with radii from Shannon (1976). The structures with nearly identical cation sizes in both sites fall on a single trend. The $CaMnSiO_4$ and $CaMgSiO_4$ trends demonstrate the effect of differences in sizes between the two octahedral sites. In $CaMnSiO_4$ the difference between the two sites is less than in $CaMgSiO_4$, so it is less distorted, but the average cation size is greater so the ideal radius is larger. The same trend is also evident in the wadsleyites. The wadsleyite with 25% Fe has both larger average cation size and greater average difference between the sites than the pure Mg phase, so it is more distorted and has a larger ideal radius. Furthermore, charge difference between the two octahedral sites appears to have no effect since $LiScSiO_4$ lies exactly where the trend predicts, based on cation sizes alone.

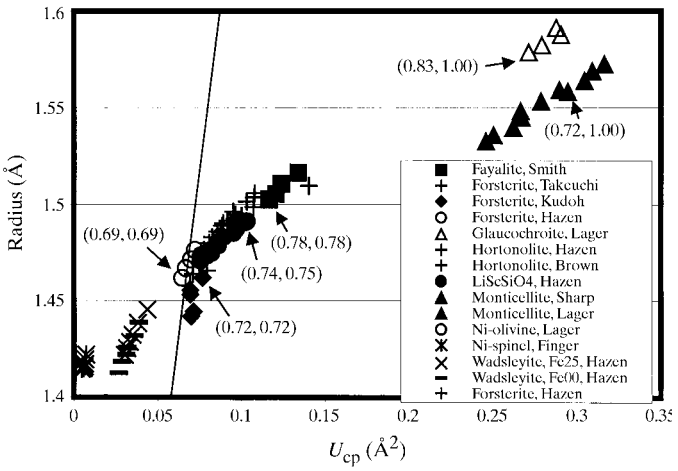

Figure 7
The relationship between the ideal radius and U_{cp}. The line shows how the radius would vary with the distortion parameter due only to scaling of the cell parameters. The numbers in parentheses are cation sizes (Shannon, 1976).

8. Conclusions

A parameter, U_{cp}, has been defined that quantifies the departure of an observed crystal structure from ideal closest-packing. By varying the radius of the spheres and the orientation of the ideal arrangement, U_{cp} can be determined for any material at temperature and pressure. Analysis of data for the pyroxenes and the $M1M2SiO_4$ polymorphs at temperature and pressure shows how anion–anion interactions play an important role in the compression and expansion of these structures. The anion skeleton moves rapidly toward ideal closest-packing with pressure. Traditional approaches provided by analysis of angle bending, bond compression, polyhedral distortions *etc.* are simply the examination of detailed features resulting from the larger scale process. Combining U_{cp} and crystal chemical data for the $M1M2SiO_4$ polymorphs shows that pressure has exactly the same effect on the structure as reducing the M-site cation sizes. We expect that further analysis of this parameter will provide valuable insights into compression and expansion mechanisms for other structures as well.

We would like to thank the National Science Foundation for funding our study, Compression Mechanisms of Upper Mantle Minerals, through grant No. EAR-9903104.

References

Angel, R. J., Gasparik, T. & Finger, L. W. (1989). *Am. Mineral.* **74**, 599–603.
Arlt, T., Angel, R. J., Miletich, R., Armbruster, T. & Peters, T. (1998). *Am. Mineral.* **83**, 1176–1181.
Benna, P., Tribaudino, M., Zanini, G. & Bruno, E. (1990). *Z. Kristallogr.* **192**, 183–199.
Berry, L. G. & Mason, B. (1959) *Mineralogy. Concepts, Descriptions, Determinations.* San Francisco: W. H. Freeman and Company.
Bragg, S. L., Claringbull, G. F. & Taylor, W. H. (1965). *Crystal Structures of Minerals.* Ithaca, New York: Cornell University Press.
Brown, G. E. (1982). *Orthosilicates, Reviews in Mineralogy*, edited by P. H. Ribbe, Vol. 5, 2nd ed., pp. 275–382. Washington, DC: Mineralogical Society of America.
Brown, G. E. & Prewitt, C. T. (1973). *Am. Mineral.* **58**, 577–587.
Brown, I. D. & Shannon, R. D. (1973). *Acta Cryst.* A**29**, 266–282.
Cameron, M., Sueno, S., Prewitt, C. T. & Papike, J. J. (1973). *Am. Mineral.* **58**, 594–618.
Clark, J. R., Appleman, D. E. & Papike, J. J. (1969). *Mineral. Soc. Am. Spec. Paper*, **2**, 31–50.
Cohen, R. E. (1994). *Silica, Physical Behavior, Geochemistry, and Materials Applications, Reviews in Mineralogy*, edited by P. J. Heaney, C. T. Prewitt and G. V. Gibbs, Vol. 29, pp. 275–382. Washington, DC: Mineralogical Society of America.
Dennis, J. E. Jr & Schnabel, R. B. (1983) *Numerical Methods for Unconstrained Optimization and Nonlinear Equations.* Englewood Cliffs, NJ: Prentice-Hall.
Dollase, W. A. (1974). *Acta Cryst.* A**30**, 513–517.
Finger, L. W. & Ohashi, Y. (1976). *Am. Mineral.* **61**, 303–310.
Finger, L. W., Hazen, R. M. & Yagi, T. (1979). *Am. Mineral.* **64**, 1002–1009.
Fleet, M. E. (1976). *Mineral. Mag.* **40**, 531–533.
Francis, C. A. & Ribbe, P. H. (1980). *Am. Mineral.* **65**, 1263–1269.
Glinneman, J., King, H. E. Jr, Schulz, H., Hahn, Th., La Placa, S. J. & Dacol, F. (1992). *Z. Kristallogr.* **198**, 177–212.

electronic reprint

Hazen, R. M. (1976). *Am. Mineral.* **61**, 1280–1293.
Hazen, R. M. (1977). *Am. Mineral.* **62,** 286–295.
Hazen, R. M. (1987). *Phys. Chem. Miner.* **14**, 13–20.
Hazen, R. M. (1999). EOS Transactions, AGU, Fall Meeting Suppl., 80 (46), F1139.
Hazen, R. M., Downs, R. T. & Finger, L. W. (1996). *Am. Mineral.* **81**, 327–334.
Hazen, R. M., Downs, R. T., Finger, L. W. & Ko, J. (1993). *Am. Mineral.* **78**, 1320–1323.
Hazen, R. M. & Finger, L. W. (1977). Annual Report of the Director, Geophysical Lab, 1976–1977, 512–515.
Hazen, R. M. & Finger, L. W. (1982). *Comparative Crystal Chemistry.* Chichester: John Wiley and Sons.
Hazen, R. M., Finger, L. W., Hemley, R. J. & Mao, H. K. (1989). *Solid State Commun.* **72**, 507–511.
Hazen, R. M., Weingerger, M. B., Yang, H. & Prewitt, C. T. (2001). *Am. Mineral.* **85**, 770–777.
Hugh-Jones, D. A., Woodland, A. B. & Angel, R. J. (1994). *Am. Mineral.* **79**, 1032–1041.
Kudoh, Y. & Takeda, H. (1986). *Physica B*, **139/140**, 333–336.
Kudoh, Y. & Takéuchi, Y. (1985). *Z. Kristallogr.* **171**, 291–302.
Lager, G. A. & Meagher, E. P. (1978). *Am. Mineral.* **63**, 365–377.
Levien, L. & Prewitt, C. T. (1981). *Am. Mineral.* **66**, 315–323.
Marumo, F., Isobe, M. & Akimoto, S. (1977). *Acta Cryst.* B**33**, 713–716.
Morimoto, N. & Güven, N. (1970). *Am. Mineral.* **55**, 1195–1209.
Morimoto, N., Tokonami, M., Watanabe, M. & Koto, K. (1974). *Am. Mineral.* **59**, 475–485.
Patterson, A. L. & Kasper, J. S. (1959). *International Tables for X-ray Crystallography*, Vol. II. Birmingham, England: Kynoch Press.
Pauling, L. (1940). *Nature of the Chemical Bond.* Ithaca, New York: Cornell University Press.
Robinson, K., Gibbs, G. V. & Ribbe, P. H. (1971). *Science*, **172**, 567–570.
Scordari, F. (1992). *Fundamentals of Crystallography*, edited by C. Giacovazzo, pp. 404–463. New York: Oxford University Press.
Shannon, R. D. (1976). *Acta Cryst.* A**32**, 751–767.
Sharp, Z. D., Hazen, R. M. & Finger, L. W. (1987). *Am. Mineral.* **72**, 748–755.
Smyth, J. R. (1975). *Am. Mineral.* **60**, 1092–1097.
Sowa, H. (1988). *Z. Kristallogr.* **184**, 257–268.
Takéuchi, Y., Takamitsu, Y., Nobuhiko, H. & Masahiro, H. (1984). *Materials Science of the Earth's Interior*, edited by I. Sunagawa, pp. 191–231. Tokyo: Terra Scientific Publishing Company.
Thompson, R. M. (2000). Master's thesis. University of Arizona, Tucson, Arizona 85721–0077, USA.
Wechsler, B. A. & Von Dreele, R. B. (1989). *Acta Cryst.* B**45**, 542–549.
Winter, J. K. & Ghose, S. (1979). *Am. Mineral.* **64**, 573–586.
Yagi, T., Marumo, F. & Akimoto, S. (1974). *Am. Mineral.* **59**, 486–490.
Yang, H., Downs, R. T., Finger, L. W., Hazen, R. M. & Prewitt, C. T. (1997). *Am. Mineral.* **82**, 467–474.
Zhang, L., Ahsbahs, H., Hafner, S. & Kutoglu, A. (1997). *Am. Mineral.* **82**, 245–258.
Zoltai, T. & Stout, J. H. (1984). *Mineralogy. Concepts and Principles.* Minneapolis, USA: Burgess Publishing Company.

electronic reprint